Journal of Materials Chemistry C

Highly efficient blue-green organic light-emitting diodes by controlling anionic migration of cationic iridium(III) complexes

Journal:	*Journal of Materials Chemistry C*
Manuscript ID	TC-ART-03-2016-001302.R1
Article Type:	Paper
Date Submitted by the Author:	27-Apr-2016
Complete List of Authors:	Ma, Dongxin; Tsinghua University, Chemistry Zhang, Chen; Tsinghua University, Chemistry Qiu, Yong; Tsinghua University, Duan, Lian; Tsinghua University,

Journal of Materials Chemistry C

PAPER

Highly efficient blue-green organic light-emitting diodes by controlling anionic migration of cationic iridium(III) complexes

Received 00th January 20xx,
Accepted 00th January 20xx

DOI: 10.1039/x0xx00000x

www.rsc.org/

Dongxin Ma, Chen Zhang, Yong Qiu and Lian Duan*

We designed and synthesized a series of cationic iridium(III) complexes with the same coordinated iridium(III) cation but different-sized counter-ions, investigated their photophysical properties, electrochemical behaviours and thermal stability, then fabricated single-layer solution-processed organic light-emitting diodes (OLEDs) thereof, and demonstrated anionic migration in devices. By doping these cationic iridium(III) complexes at low concentrations (2 or 3 wt. %) thus avoiding their anionic migration, we succeeded in the preparation of efficient blue-green OLEDs, achieving a highest current efficiency of 17.1 cd A^{-1}, external quantum efficiency of 6.8 %, maximum luminance of 14.2×10^3 cd m^{-2} and colour coordinates of (0.21, 0.48). To our knowledge, these values are among the best reported OLEDs based on ionic transition metal complexes as phosphorescent emitters in the blue-green region. Impact of different-sized counter-ions on carrier transport characteristics were also examined by single carrier devices. Notably, by doping these cationic iridium(III) complexes at high concentrations (20 wt. %) thus wisely employing their anionic migration, we developed simple-constructed OLEDs with temporary *p-i-n* junction instead of active *n*-type dopants in the cathode and obtained a high current efficiency of 8.3 cd A^{-1} and maximum luminance of 12.8×10^3 cd m^{-2}, rather comparable to the corresponding OLEDs with conventional Cs_2CO_3 active cathode.

Introduction

Organic electroluminescence is a promising technology for flat-panel displays and solid-state lighting, especially organic light-emitting diodes (OLEDs), which motivates intensive efforts to develop various kinds of emitters.[1] In OLEDs, electrically injected charge carriers recombine to produce singlet and triplet excitons in a 1:3 ratio, according to spin statistics.[2] For early devices based on fluorescent dyes, only the singlet spin states induce photons, so the efficiency is limited to 25 % in theory.[3] Afterwards the use of phosphorescent dopants exploits the normally non-radiative triplet excitons thus offers a means of achieving improved light-emission efficiency.[4-5]

Heavy metal complexes with effective intersystem crossing are widely used as phosphorescent materials for OLEDs.[6-9] Among them, trivalent iridium complexes with easily tunable colours by independent chemical modifications of the ligands and remarkable photophysical properties,[10] are by far the most favourable triplet emitters, while neutral in most cases before.[11-17] Only until Plummer *et al.* reported the first example of OLEDs based on yellow-emitting charged iridium dyes in 2005,[18] cationic iridium(III) complexes with many merits such as ease of synthesis, excellent luminescent properties and emission of virtually all colours, have emerged as promising phosphors for OLEDs and attracted intense interest.[19-26] However, most of the previously demonstrated cationic iridium(III) complexes contain emissive coordinated iridium(III) cations and nonluminous small negative counter-ions such as tetrafluoroborate ($[BF_4]^-$) and hexafluorophosphate ($[PF_6]^-$), of which the charged nature and easy migration always complicate operation of the devices, thus deep understanding of this process still remains challenging.

In this paper we developed a series of cationic iridium(III) complexes with the same coordinated iridium(III) cation but different-sized counter-ions, conventional $[BF_4]^-$, $[PF_6]^-$ and other two bulky tetraphenylborate-type negative counter-ions, tetrakis(pentafluorophenyl)borate ($[B(5fph)_4]^-$) and tetrakis[3,5-bis(trifluoromethyl)phenyl]borate ($[BArF_{24}]^-$), respectively. By using these novel phosphorescent materials with varied doping concentrations thus controlling their anionic migration, we produced and evaluated highly efficient solution-processed OLEDs. Our results provide a new insight into OLEDs based on charged materials, which is essential for the development of robust and high performance organic electronics.

Results and discussion

Synthesis and structural characterization.

*Key Lab of Organic Optoelectronics and Molecular Engineering of Ministry of Education, Department of Chemistry, Tsinghua University, Beijing 100084, P. R. China. *E-mail: duanl@mail.tsinghua.edu.cn; Fax: +86-10-62795137; Tel: +86-10-62788802.*

† Electronic Supplementary Information (ESI) available: [Synthetic routes, single crystal structures, absorption spectra, molecular orbital surfaces and device characteristics]. See DOI: 10.1039/x0xx00000x

As depicted in **Figure 1**, complexes 1-4 share the same coordinated iridium(III) cation $[Ir(ppy)_2(pzpy)]^+$, while different-sized negative counter-ions $[BF_4]^-$, $[PF_6]^-$, $[B(5fph)_4]^-$ and $[BArF_{24}]^-$, respectively. Here ppy is 2-phenylpyridine and pzpy is 2-(1*H*-pyrazol-1-yl) pyridine. Synthetic routes of both the ligands and complexes are described in **Scheme S1** (see Electronic Supplementary Information).

To gain insights into the structural features, we successfully grew single crystals of complexes 1-4 from mixed solution and investigated their characteristics by X-ray diffraction crystallography (see Experimental Section and **Figures S1-S4**). In agreement with the previous literatures on cationic iridium(III) complexes,[27,28] $[Ir(ppy)_2(pzpy)]^+$ shows distorted octahedral geometries around the trivalent iridium center with two cyclometalated ligands adopting *C,C-cis, N,N-trans* configurations. $[PF_6]^-$ demonstrates an octahedral geometry around the phosphorus atom, while $[BF_4]^-$, $[B(5fph)_4]^-$ and $[BArF_{24}]^-$ exhibit regular tetrahedron geometries around the boron core. Quantum chemical calculation results based on these structural data indicate that anionic volume of $[BF_4]^-$, $[PF_6]^-$, $[B(5fph)_4]^-$ and $[BArF_{24}]^-$ increases from 35.25, 49.95, 320.78 to 425.02 cm^3 mol^{-1}, respectively.

<Figure 1>

Physicochemical properties.

Photophysical properties of complexes 1-4 are presented in **Figure 2a-b** and summarized in **Table 1**. Seen from the absorption spectra in **Figure S5**, the intense bands in the ultra-violet region peaked at ca. 260 nm are attributed to spin-allowed $^1\pi$-π^* transitions from the ligands, while the relatively weaker bands between 350 to 450 nm are ascribed to excitations to ^{1}MLCT (metal-to-ligand charge-transfer), ^{1}LLCT (ligand-to-ligand charge-transfer), ^{3}MLCT, ^{3}LLCT and ligand-centered (LC) $^3\pi$-π^* transitions. Quantum chemical calculations performed on the basis of the geometries obtained from single crystal structures further demonstrated that the LLCT transitions correspond to electron promotions from the phenyl groups of ppy ligands to pzpy ligands (see **Figure S6**). And the spin-forbidden ^{3}MLCT, ^{3}LLCT and LC $^3\pi$-π^* transitions also gain high intensity by mixture with the higher-lying ^{1}MLCT transition through spin-orbit coupling endowed by the heavy iridium atom.[29] In dilute acetonitrile solution, complexes 1-4 phosphoresce green-blue with a major emission peak at ca. 475 nm and a shoulder peak at 503 nm, independent of counter-ions. The vibronically structured emission at 77 K and room temperature (RT) indicate that their emissive excited states have predominantly ^{3}LC π-π^* rather than ^{3}LLCT or ^{3}MLCT characters, which always exhibit broad and featureless emission spectra.[30,31] It is worth mentioning that photoluminescence (PL) spectra of complexes in solid state are quite different from those in solution. In the 5 wt. % doped polymethylmethacrylate (PMMA) thin film, complex 1 shows green-blue emission peaked at 479 nm with a shoulder at 507 nm, while the peak wavelength of complexes 2-4 is a little blue-shifted. By contrast, PL spectra of complexes 1-4 in neat film are peaked at 487, 483, 476 and 473 nm, respectively. This obvious blue shift can be explained by the increasing steric hindrance of counter-ions. In solid state, larger-sized counter-ions show a weaker electric field, probably decreasing the angles of ligands (ppy and pzpy) plane in the coordinated iridium(III) cation and increasing tensile force between ligands, thus are less able to stabilize the polar excited states and cause the blue shift. PLQYs of complexes 3 and 4 in neat film reach 0.40, much higher than that of complex 1 (0.02) and 2 (0.03), according with our previous work.[32]

Electrochemical behaviours of complexes 1-4 were then probed by cyclic voltammetry in degassed acetonitrile solution. As shown in **Figure 2c** and **Table 1**, the redox potentials of complexes 1-4 are rather similar with a reduction potential of ca. -2.2 V and an oxidation potential of ca. 0.9 V, excluding the influence of redox on the devices.[33]

In addition, thermogravimetric analysis (TGA) under nitrogen flow shows that complexes 1-4 are thermally stable with the 5 % weight reduction temperatures all over 300 °C (see **Figure 2d**).

<Figure 2>

<Table 1>

Single-layer solution-processed OLEDs.

To explore electroluminescent (EL) characteristics of complexes 1-4, we fabricated single-layer solution-processed OLEDs thereof, with a following structure of ITO/ PEDOT: PSS (60 nm)/ PVK: OXD-7: *x* wt. % Emitter (85 nm)/ Cs_2CO_3 (2.3 nm)/ Al (150 nm), and *x* was varied from 2 to 20 %, as shown in **Figure 3a**. Here poly(3,4-ethylenedioxythiophene): poly(styrene sulfonate) (PEDOT: PSS) layer was spin-coated from deionized water in air at 3000 rpm then annealed at 200 °C to yield a 60 nm smooth film as the hole injection layer, the light-emitting layer consisting of poly(*N*-vinylcarbazole) (PVK) host, 1,3-bis(5-(4-*tert*-butylphenyl)-1,3,4-oxadiazol-2-yl)benzene (OXD-7) as electron transport material and phosphorescent dopant was cast from 1,2-dichloroethane at 1500 rpm in a glove box filled with nitrogen then baked at 80 °C to form an 85 nm emissive film. Finally Cs_2CO_3/Al was fabricated thereon as an active metal cathode by vacuum evaporation deposition. Molecular structures and energy level diagram of the materials mentioned are also described in **Figure 3a**, with device characteristics shown in **Figure 3b-d** and details tabulated in **Table 2**.

<Figure 3>

Seen from **Figures S7-10**, OLEDs doped with different concentrations of complexes 1-4 show blue-green emission with quite similar PL and EL spectra. The major peak was centered at ca. 482 nm with a shoulder at ca. 508 nm, and Commission International de l'Eclairage (CIE) coordinates vary a little from (0.20, 0.46) to (0.24, 0.49). The red-shifted EL spectra of devices doped with high concentration of phosphorescent emitters may be explained by the polarization effect of the molecular orbitals under the high electric field in these devices.[35]

As shown in **Table 2**, OLEDs based on low concentrations of complexes 1-4 show excellent performance. Using 2 %

complex 1, we attained a high current efficiency of 14.8 cd A^{-1} and maximum brightness of 12.5×10^3 cd m^{-2}. With 3 % complex 2, the current efficiency and luminance are even higher, up to 17.1 cd A^{-1} and 14.2×10^3 cd m^{-2}, respectively, among the best performance of OLEDs based on ionic transition metal complexes (see **Table S1**).[18-24,36,37] Employing 3 % complex 3 or 2 % complex 4, we also obtained desirable device performance with a maximum current efficiency of 13.6 and 12.4 cd A^{-1}, respectively. However, turn-on voltages of these OLEDs are a little higher than those based on neutral iridium(III) complexes, due to the electron trap of charged emitters.[18]

Figure S7a-b depicted current density (*J*) and luminance (*L*) *versus* voltage (*V*) characteristics of devices based on varied concentrations of complex 1. We noticed that *J*-*V* curves shifted towards the low voltages. *J* of devices doping with low ratios of complex 1 is high, J_1 (2 %) at 15 V reaches 3089 A m^{-2}, J_1 (3 %) is 2471 A m^{-2} and J_1 (5 %) is 2197 A m^{-2}, whereas that of devices doping with high ratios is much lower, J_1 (10 %) is 720 A m^{-2}, J_1 (15 %) is 565 A m^{-2} and J_1 (20 %) is only 346 A m^{-2}, nearly 11 % of J_1 (2 %). *L*-*V* curves also shifted towards the lower *V*, while OLEDs based on different ratios of complex 1 feature similar maximum *L*. Analogous phenomena were also observed for devices based on complexes 2-4 (see **Figures S8-S10**), especially for complex 2. As described in **Figure S8a-b**, J_2 (2 %) at 15 V is as high as 1201 A m^{-2}, while J_2 (3 %) is 774 A m^{-2} and J_2 (5 %) is only 245 A m^{-2}. Along with the increasing doping ratios, *J* decreases quite sharply. J_2 (10 %) is 128 A m^{-2}, while J_2 (15 %) is 19 A m^{-2} and J_2 (20 %) is only 0.7 A m^{-2}, even less than 0.06 % of J_2 (2 %). Consequently, devices doping with 2 to 10 % complex 2 show a high *L* over 10^4 cd m^{-2}, while the maximum luminance of devices based on 15 % or 20 % complex 2 is quite low. Max L_2 (15 %) is 2.3×10^3 cd m^{-2}, and max L_2 (20 %) is only 275 cd m^{-2}. Seen from **Figures S9-S10**, *J* also decreases in the devices doping with increasing concentrations of complexes 3-4, while the variation range is much smaller than that of devices based on complex 2. *J* of the device doping with 20 % complex 3, J_3 (20 %) is 10 A m^{-2} at 15 V, nearly 2.4 % of J_3 (2 %), 424 A m^{-2}. Maximum luminance of the device based on 20 % complex 3, max L_3 (20 %) is 1.4×10^3 cd m^{-2}, quite higher than max L_2 (20 %). Furthermore, current density of the device doping with 20 % complex 4, J_4 (20 %) is 33 A m^{-2} at 15 V, about 4.0 % of J_4 (2 %), 816 A m^{-2}. Maximum luminance of the device based on 20 % complex 4, max L_4 (20 %) is 5.7×10^3 cd m^{-2}, almost the same with that of the device based on 2 % complex 4, max L_4 (2 %).

This evident variation in *J* and the relevant *L* can be explained by the migration of different-sized negative counter-ions (*i.e.*, anionic migration) in devices based on cationic iridium(III) complexes at the working bias (vide infra).

Anionic migration and OLEDs with *p*-*i*-*n* junction.

In order to further understand the effect of counter-ions on carrier transport characteristics in devices, we then fabricated single carrier devices based on complexes 1-4 by solution-based processing. The structure of hole-only device is ITO/ PEDOT: PSS (60 nm)/ PVK: OXD-7: *x* wt. % Emitter (85 nm)/ Al (150 nm), while that of electron-only device is ITO/ PVK: OXD-7: *x* wt. % Emitter (85 nm)/ Cs_2CO_3 (2.3 nm)/ Al (150 nm). For complex 1 or 4, *x* =2 and for complex 2 or 3, *x* = 3, consistent with the optimized doping ratio for OLEDs.

As described in **Figure 4**, current density of hole- and electron-only devices is well matched, indicating a balanced charge transport in the corresponding light-emitting devices. Note that *J* decreases from complexes 1 to 4, in relation to the different-sized counter-ions. For complexes 1-2, *J* of hole-only device is a little lower than that of electron-only device, while for complexes 3-4, the latter is higher. Under the working bias, coordinated iridium(III) cations and anions move then accumulate adjacent to the cathode and anode, to create an *n*-doped or *p*-doped layer, respectively, forming a temporary *p*-*i*-*n* junction. In devices based on complexes 1 and 2, the small counter-ions $[BF_4]^-$ and $[PF_6]^-$ move much faster than the bulky coordinated iridium cation $[Ir(ppy)_2(pzpy)]^+$, so the electron-only device exhibits a higher *J* than the hole-only device. While in single carrier devices based on complexes 3 and 4, migration rate of $[B(5fph)_4]^-$ and $[BArF_{24}]^-$ is quite reduced by their large steric hindrance, even slower than $[Ir(ppy)_2(pzpy)]^+$, leading to a lower *J* for electron-only devices than hole-only devices.

<Figure 4>

Moreover, as it is known, alkali metals from their precursors have been widely used as *n*-type dopants into the cathode of OLEDs to improve the device charge transport thus reduce the operation voltage. However, their high reactivity and diffusivity always lead to inferior device stability in the presence of ambient oxygen or water, and severe exciton quenching in the emitting layers.[38, 39] To address this problem, here we employed anionic migration to develop simple-constructed OLEDs with this temporary *p*-*i*-*n* junction instead of the active Cs_2CO_3 *n*-type layer. The device structure is ITO/ PEDOT: PSS (60 nm)/ PVK: OXD-7: 20 wt. % Emitter (85 nm)/ Al (150 nm). Experiments indicate that devices based on complexes 1-2 are turned-on below 15 V, owing to the fast anionic migration of small counter-ions, while those based on complexes 3-4 are not, as described in **Figure 5**. Note that the device based on complex 1 was turned on at only 9.6 V, achieving a high current efficiency of 8.3 cd A^{-1} and maximum luminance of 12.8×10^3 cd m^{-2}, rather comparable to the corresponding OLEDs with conventional Cs_2CO_3 active cathode, of which the maximum current efficiency and luminance is 8.6 cd A^{-1} and 12.5×10^3 cd m^{-2}, respectively (see **Table 2**). It is the first work to employ ionic emitters as both phosphorescent dyes and *n*-type dopants, indicating their probable applications in solution-processed OLEDs.

<Figure 5>

<Table 2>

Conclusions

In summary, we reported a series of cationic iridium(III) complexes with the same emissive coordinated iridium(III) cation but different-sized nonluminous negative counter-ions, investigated their physicochemical properties, then fabricated

and evaluated single-layer solution-processed OLEDs thereof. We found that both current density and luminance were reduced along with increasing doping concentrations of these charged phosphorescent emitters, due to their anionic migration in devices. By optimization of doping concentrations thus controlling the anionic migration, we obtained single-layer devices with a highest current efficiency of 17.1 cd A^{-1}, external quantum efficiency of 6.8 % and maximum brightness of 14.2×10^3 cd m^{-2}, among the best reported OLEDs based on ionic transition metal complexes in the blue-green region. What is more, we developed simple-constructed OLEDs with the temporary *p-i-n* junction owing to anionic migration of the cationic iridium(III) complexes, achieving a high current efficiency of 8.3 cd A^{-1} and maximum luminance of 12.8×10^3 cd m^{-2}, rather comparable to the corresponding OLEDs with Cs_2CO_3 active cathode, indicating the promising potential of ionic emitters in OLEDs, not only as phosphorescent dyes, but also as *n*-type dopants. We believe this work may help understanding the operation and dynamics of OLEDs based on charged materials, while quantitative assessment of the charge transport characteristics in devices remains an open aspect of further research.

Experimental

Materials.

Unless otherwise stated, all the reactants and solvents were purchased from commercial sources and used. The pzpy ligand and dichloro-bridged diiridium complexes $[Ir(ppy)_2Cl]_2$ were synthesized according to our previous literature.[34]

Synthesis and characterization of complex 1.

$[Ir(ppy)_2Cl]_2$ (0.802 g, 0.75 mmol) and pzpy ligand (0.236 g, 1.63 mmol) were dissolved in 1,2-ethanediol (60 mL) and then refluxed at 140 °C for 13 h under an argon atmosphere to form a clear bright yellow solution. After cooling to room temperature, an aqueous solution of $NaBF_4$ (1.046 g, 9.53 mmol) was slowly added into the reaction mixture under stirring, resulting in a yellow suspension. After filtration, the suspension was dried under vacuum at 70 °C overnight. The crude product was purified by column chromatography on silica gel (200-300 mesh) with CH_2Cl_2/ MeOH (*v*/*v* = 10:1) as the eluent, yielding a bright yellow powder (0.845 g, 1.15 mmol). Yield: 77 %.^{1}H-NMR (600 MHz, DMSO-d_6) δ 9.30 (d, *J* = 3.0 Hz, 1H), 8.52 (d, *J* = 8.4 Hz, 1H), 8.35-8.31 (m, 1H), 8.26 (dd, *J* = 8.1, 3.7 Hz, 2H), 7.95 (ddd, J = 9.7, 2.5, 1.2 Hz, 2H), 7.89 (dd, *J* = 12.6, 7.8 Hz, 2H), 7.76 (d, *J* = 5.7 Hz, 1H), 7.71 (d, *J* = 5.7 Hz, 1H), 7.64 (d, *J* = 5.4 Hz, 1H), 7.53 (t, J = 6.6 Hz, 1H), 7.28 (d, *J* = 1.9 Hz, 1H), 7.22 (dd, *J* = 9.7, 3.6 Hz, 1H), 7.18 (dd, *J* = 9.7, 3.6 Hz, 1H), 7.01 (t, *J* = 7.5 Hz, 1H), 6.97 (t, *J* = 7.5 Hz, 1H), 6.9-6.87 (m, 2H), 6.84 (dd, *J* = 10.7, 4.2 Hz, 1H), 6.18 (t, *J* = 8.4 Hz, 2H); ^{19}F-NMR (600 MHz, DMSO-d_6) δ -148.14 (s, 4F); MS (ESI) [*m/z*]: $[M\text{-}BF_4]^+$ calcd for $C_{30}H_{23}IrN_5$, 646.16; found, 646.16; $[M\text{-}Ir(ppy)_2(pzpy)]^-$ calcd for BF_4, 87.00; found, 87.00. Single crystal was grown from acetone / methanol mixed solution and characterized by X-ray crystallography. Space group of P_{bca} with *a* = 10.625(2) Å, *b* = 15.478(3) Å, *c* = 32.301(7) Å, α = 90.00 °, β = 90.00 °, γ = 90.00 °, *V* = 5312.0(18) Å^3, *Z* = 8, d_{calcd} = 1.8114 g cm^{-3}, R_1 = 0.0898, ωR_2 = 0.2274 for 6053 observed reflections [$I \geq 2\sigma(I)$] (CCDC 1469391).

Synthesis and characterization of complex 2.

The synthetic route of complex 2 is quite similar to that of complex 1 except that $NaBF_4$ was replaced with NH_4PF_6. Yield: 89 %. ^{1}H-NMR (600 MHz, DMSO-d_6) δ 9.32 (d, *J* = 3.0 Hz, 1H), 8.54 (d, *J* = 8.5 Hz, 1H), 8.35 (td, *J* = 8.5, 1.6 Hz, 1H), 8.28 (dd, *J* = 8.0, 3.7 Hz, 2H), 8.00-7.96 (m, 2H), 7.92 (d, *J* = 7.6 Hz, 1H), 7.90 (d, *J* = 7.4 Hz, 1H), 7.78 (dd, *J* = 6.0, 0.6 Hz, 1H), 7.73 (dd, *J* = 5.8, 0.6 Hz, 1H), 7.67 (dd, *J* = 5.5, 0.7 Hz, 1H), 7.57-7.54 (m, 1H), 7.30 (d, *J* = 2.0 Hz, 1H), 7.26-7.19 (m, 2H), 7.05-6.99 (m, 2H), 6.93 (dd, *J* = 2.9, 2.1 Hz, 1H), 6.91 (dd, *J* = 7.4, 1.0 Hz, 1H), 6.87 (td, *J* = 7.6, 1.1 Hz, 1H), 6.21 (dd, *J* = 9.5, 8.1 Hz, 2H); ^{19}F-NMR (600 MHz, DMSO-d_6) δ -69.92 (s, 3F), -71.22 (s, 3F); MS (ESI) [*m/z*]: $[M\text{-}PF_6]^+$ calcd for $C_{30}H_{23}IrN_5$, 646.16; found, 646.16; $[M\text{-}Ir(ppy)_2(pzpy)]^-$ calcd for PF_6, 144.96; found, 144.96. Single crystal was grown from acetonitrile solution and characterized by X-ray crystallography. Space group of P_{bca} with *a* = 10.9764(6) Å, *b* = 15.8495(9) Å, *c* = 33.0276(18) Å, α = 90.00 °, β = 90.00 °, γ = 90.00 °, *V* = 5745.8(6) Å^3, *Z* = 8, d_{calcd} = 1.828 g cm^{-3}, R_1 = 0.0436, ωR_2 = 0.0816 for 6592 observed reflections [$I \geq 2\sigma(I)$] (CCDC 680949).

Synthesis and characterization of complex 3.

The synthetic route of complex 3 is quite similar to that of complex 1 except that $NaBF_4$ was replaced with $Na[B(5fph)_4]$. Yield: 72 %. ^{1}H-NMR (600 MHz, DMSO-d_6) δ 9.28 (d, *J* = 2.8 Hz, 1H), 8.51 (d, *J* = 8.3 Hz, 1H), 8.31 (t, *J* = 8.0 Hz, 1H), 8.28-8.21 (m, 2H), 7.94 (d, *J* = 7.8 Hz, 2H), 7.88 (dd, *J* = 12.3, 7.8 Hz, 2H), 7.75 (d, *J* = 5.7 Hz, 1H), 7.70 (d, *J* = 5.6 Hz, 1H), 7.64 (d, *J* = 5.5 Hz, 1H), 7.54-7.50 (m, 1H), 7.27 (s, 1H), 7.25-7.15 (m, 2H), 6.99 (dt, *J* = 19.2, 7.5 Hz, 2H), 6.93-6.80 (m, 3H), 6.22-6.15 (m, 2H); ^{19}F-NMR (600 MHz, DMSO-d_6) δ -132.35 (s, 8F), -161.20 (s, 4F), -165.81 (s, 8F); MS (ESI) [*m/z*]: $[M\text{-}B(5fph)_4]^+$ calcd for $C_{30}H_{23}IrN_5$, 646.16; found, 646.40; $[M\text{-}Ir(ppy)_2(pzpy)]^-$ calcd for $C_{24}BF_{20}$, 678.98; found, 679.22. Single crystal was grown from acetone / deionized water mixed solution and characterized by X-ray crystallography. Space group of $C_{2/c}$ with *a* = 36.085(7) Å, *b* = 17.076(3) Å, *c* = 17.762(4) Å, α = 90.00 °, β = 110.34(3) °, γ = 90.00 °, *V* = 10263(4) Å^3, *Z* = 8, d_{calcd} = 1.798 g cm^{-3}, R_1 = 0.0477, ωR_2 = 0.1102 for 9695 observed reflections [$I \geq 2\sigma(I)$] (CCDC 992099).

Synthesis and characterization of complex 4.

The synthetic route of complex 4 is quite similar to that of complex 1 except that $NaBF_4$ was replaced with $Na[BArF_{24}]$. Yield: 81 %. ^{1}H-NMR (600 MHz, DMSO-d_6) δ 9.30 (d, *J* = 3.0 Hz, 1H), 8.53 (d, *J* = 8.5 Hz, 1H), 8.35-8.30 (m, 1H), 8.26 (dd, *J* = 8.0 Hz, 3.9 Hz, 2H), 7.95 (ddd, *J* = 7.7 Hz, 3.2 Hz, 1.9 Hz, 2H), 7.89 (dd, *J* = 12.6 Hz, 7.8 Hz, 2H), 7.77 (d, *J* = 5.7 Hz, 1H), 7.71 (d, *J* = 5.3 Hz, 1H), 7.68 (s, 4H), 7.65 (d, *J* = 5.6 Hz, 1H), 7.61 (s, 8H), 7.55-7.51 (m, 1H), 7.28 (d, *J* = 1.9 Hz, 1H),

7.22 (t, *J* = 6.7 Hz, 1H), 7.18 (t, *J* = 6.6 Hz, 1H), 7.01 (t, *J* = 8.0 Hz, 1H), 6.98 (t, *J* = 7.5 Hz, 1H), 6.91-6.87 (m, 2H), 6.84 (t, *J* = 7.4 Hz, 1H), 6.19 (dd, *J* = 9.6 Hz, 7.9 Hz, 2H); ^{19}F-NMR (600 MHz, DMSO-d_6) δ -61.74 (s, 24F); MS (ESI) [*m/z*]: $[M\text{-}BArF_{24}]^+$ calcd for $C_{30}H_{23}IrN_5$, 646.16; found, 646.16; $[M\text{-}Ir(ppy)_2(pzpy)]^-$ calcd for $C_{32}H_{12}BF_{24}$, 863.06; found, 863.06. Single crystal was grown from acetone / deionized water mixed solution and characterized by X-ray crystallography. Space group of $P2_{1/n}$ with a = 13.363(3) Å, b = 53.158(11) Å, c = 17.967(4) Å, α = 90.00 °, β = 108.99(3) °, γ = 90.00 °, V = 12068(4) Å^3, Z = 4, d_{calcd} = 1.698 g cm^{-3}, R_1 = 0.0696, ωR_2 = 0.1214 for 20705 observed reflections [$I \geq 2\sigma(I)$] (CCDC 992098).

More detailed data of the mentioned single crystal structures can be obtained free from the Cambridge Crystallographic Data Centre from www.ccdc.cam.ac.un/conts/retrieving.html.

Acknowledgements

We would like to thank the National Natural Science Fund for Distinguished Young Scholars of China (Grant No. 51525304), the National Key Basic Research and Development Program of China (Grant No. 2015CB655002) for financial support. We are grateful to Prof. Yongge Wei from Tsinghua University for his kind help with single crystal structural analysis.

Notes and references

1 C. W. Tang and S. A. VanSlyke, *Appl. Phys. Lett.*, 1987, **51**, 913.
2 L. J. Rothberg and A. J. Lovinger, *J. Mater. Res.,* 1996, **11**, 3174.
3 M. Pope, H. P. Kallmann and P. Magnante, *J. Chem. Phys*., 1963, **38**, 2042.
4 M. A. Baldo, D. F. O'Brien, Y. You, A. Shoustikov, S. Sibley, M. E. Thompson and S. R. Forrest, *Nature,* 1998, **395**, 151.
5 M. A. Baldo, S. Lamansky, P. E. Burrows, M. E. Thompson, and S. R. Forrest, *Appl. Phys. Lett.,* 1999, **75**, 4.
6 P. -T. Chou and Y. Chi, *Chem. Eur. J.* 2007, **13**, 380.
7 G. Cheng, S. C. F. Kui, W. -H. Ang, M. -Y. Ko, P. -K. Chow, C. -L. Kwong, C. -C. Kwok, C. Ma, X. Guan, K. -H. Low, S. -J. Su and C. -M. Che, *Chem. Sci.*, 2014, **5**, 4819.
8 A. F. Henwood, M. Lesieur, A. K. Bansal, V. Lemaur, D. Beljonne, D. G. Thompson, D. Graham, A. M. Z. Slawin, I. D. W. Samuel, C. S. J. Cazin and E. Z. Colman, *Chem. Sci.*, 2015, **6**, 3248.
9 D. Escudero, *Chem. Sci.*, 2016, **7**, 1262.
10 R. D. Costa, E. Ortí, H. J. Bolink, F. Monti, G. Accorsi and N. Armaroli, *Angew. Chem. Int. Ed.,* 2012, **51**, 8178.
11 C. Adachi, M. A. Baldo, S. R. Forrest, S. Lamansky, M. E. Thompson and R. C. Kwong, *Appl. Phys. Lett.,* 2001, **78**, 1622.
12 R. J. Holmes, S. R. Forrest, Y. -J. Tung, R. C. Kwong, J. J. Brown, S. Garon and M. E. Thompson, *Appl. Phys. Lett.,* 2003, **82**, 2422.
13 S. -J. Yeh, M. -F. Wu, C. -T. Chen, Y. -H. Song, Y. Chi, M. -H. Ho, S. -F. Hsu and C. H. Chen, *Adv. Mater.,* 2005, **17**, 285.
14 C. -F. Chang, Y. -M. Cheng, Y. Chi, Y. -C. Chiu, C. -C. Lin, G. -H. Lee, P. -T. Chou, C. -C. Chen, C. -H. Chang and C. -C. Wu, *Angew. Chem. Int. Ed.,* 2008, **47**, 4542.
15 D. Xia, B. Wang, B. Chen, S. Wang, B. Zhang, J. Ding, L. Wang, X. Jing and F. Wang, *Angew. Chem. Int. Ed.,* 2014, **53**, 1048.
16 X. Wang, S. Wang, Z. Ma, J. Ding, L. Wang, X. Jing and F. Wang, *Adv. Funct. Mater.,* 2014, **24**, 3413.
17 Y. Wang, S. Wang, N. Zhao, B. Gao, S. Shao, J. Ding, L. Wang, X. Jing and F. Wang, *Polym. Chem.*, 2015, **6**, 1180.
18 E. A. Plummer, A. Dijken, H. W. Hofstraat, L. D. Cola and K. Brunner, *Adv. Funct. Mater.,* 2005, **15**, 281.
19 W. -Y. Wong, G. -J. Zhou, X. -M. Yu, H.-S. Kwok and Z. Lin, *Adv. Funct. Mater.,* 2007, **17**, 315.
20 L. He, L. Duan, J. Qiao, D. Zhang, G. Dong, L. Wang and Y. Qiu, *Org. Electronics.,* 2009, **10**, 152.
21 L. He, L. Duan, J. Qiao, D. Zhang, L. Wang and Y. Qiu, *Org. Electronics.,* 2010, **11**, 1185.
22 B. Park, Y. H. Huh, H. G. Jeon, C. H. Park, T. K. Kang, B. H. Kim, and J. Park, *J. Appl. Phys.,* 2010, **108**, 094506.
23 G. Nasr, A. Guerlin, F. Dumur, L. Beouch, E. Dumas, G. Clavier, F. Miomandre, F. Goubard, D. Gigmes, D. Bertin, G. Wantz and C. R. Mayer, *Chem. Commun.,* 2011, **47**, 10698.
24 H. Tang, Y. Li, B. Zhao, W. Yang, H. Wu and Y. Cao, *Org. Electronics.* 2012, **13**, 3211.
25 M. Sessolo, D. Tordera and H. J. Bolink, *ACS Appl. Mater. Interfaces,* 2013, **5**, 630.
26 F. Zhang, D. Ma, L. Duan, J. Qiao, G. Dong, L. Wang and Y. Qiu, *Inorg. Chem.,* 2014, **53**, 6596.
27 J. D. Slinker, A. A. Gorodetsky, M. S. Lowry, J. Wang, S. Parker, R. Rohl, S. Bernhard and G. G. Malliaras, *J. Am. Chem. Soc.*, 2004, **126**, 2763.
28 M. S. Lowry, W. R. Hudson, R. A. Pascal Jr. and S. Bernhard, *J. Am. Chem. Soc.,* 2004, **126**, 14129.
29 M. G. Colombo, T. C. Brunold, T. Riedener, H. U. Güdel, M. Förtsch and H. B. Bürgi, *Inorg. Chem.*, 1994, **33**, 545.
30 M. G. Colombo and H. U. Güdel, *Inorg. Chem.,* 1993, *32*, 3081.
31 M. G. Colombo, A. Hauser, H. U. Güdel, *Inorg. Chem.,* 1993, **32**, 3088.
32 D. Ma, L. Duan, Y. Wei, L. He, L. Wang and Y. Qiu, *Chem. Commun.,* 2014, **50**, 530.
33 D. Ma, L. Duan, Y. Wei and Y. Qiu, *Chem. Eur. J.,* 2014, **20**, 15903.
34 L. He, L. Duan, J. Qiao, R. Wang, P. Wei, L. Wang and Y. Qiu, *Adv. Funct. Mater.,* 2008, **18**, 2123.
35 Y. -M. Wang, F. Teng, Y. -B. Hou, Z. Xu, Y. -S. Wang and W. -F. Fu, *Appl. Phys. Lett.,* 2005, **87**, 233512.
36 B. Carlson, G. D. Phelan, W. Kaminsky, L. Dalton, X. Jiang, S. Liu and A. K. -Y. Jen, *J. Am. Chem. Soc.*, 2002, **124**, 14162.
37 Q. Zhang, Q. Zhou, Y. Cheng, L. Wang, D. Ma, X. Jing and F. Wang, *Adv. Mater.*, 2004, **16**, 432.
38 B. D. Naab, S. Zhang, K. Vandewal, A. Salleo, S. Barlow, S. R. Marder and Z. Bao, *Adv. Mater.*, 2014, **26**, 4268.
39 Z. Bin, L. Duan and Y. Qiu, *ACS Appl. Mater. Interfaces*, 2015, **7**, 6444.

Figure 1. Chemical structures of complexes 1-4 with different-sized negative counter-ions.

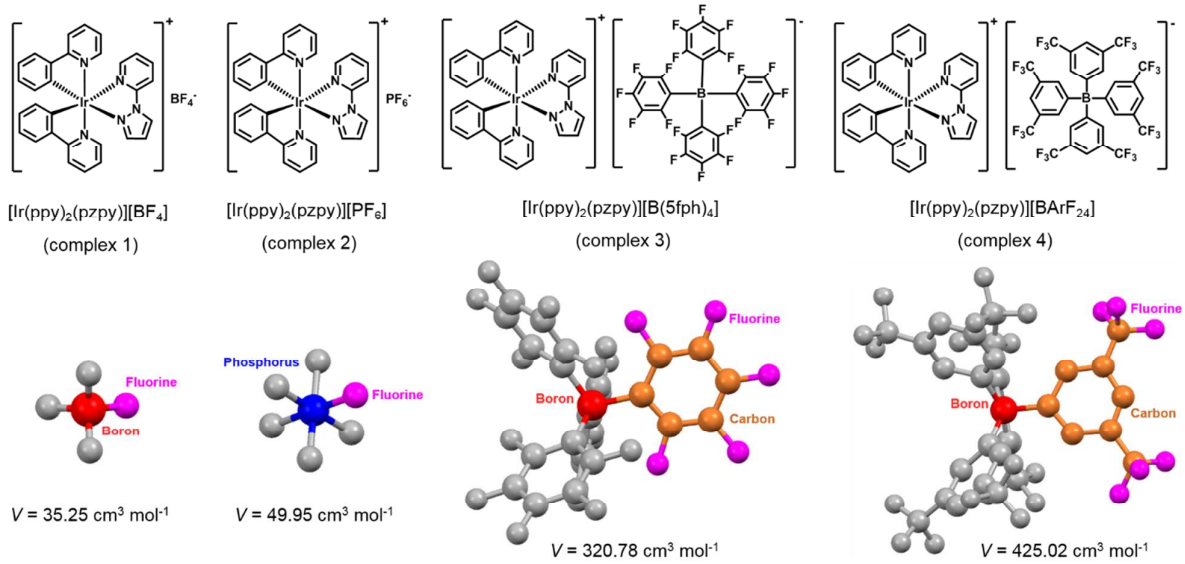

Figure 2. Photophysical properties, electrochemical behaviours and thermal stability of complexes 1-4. (a) PL spectra at 77 K and RT in acetonitrile solution, (b) PL spectra of 5 wt. % doped PMMA film and neat film, (c) cyclic voltammogram in degassed acetonitrile solution and (d) thermogravimetric analysis under nitrogen flow.

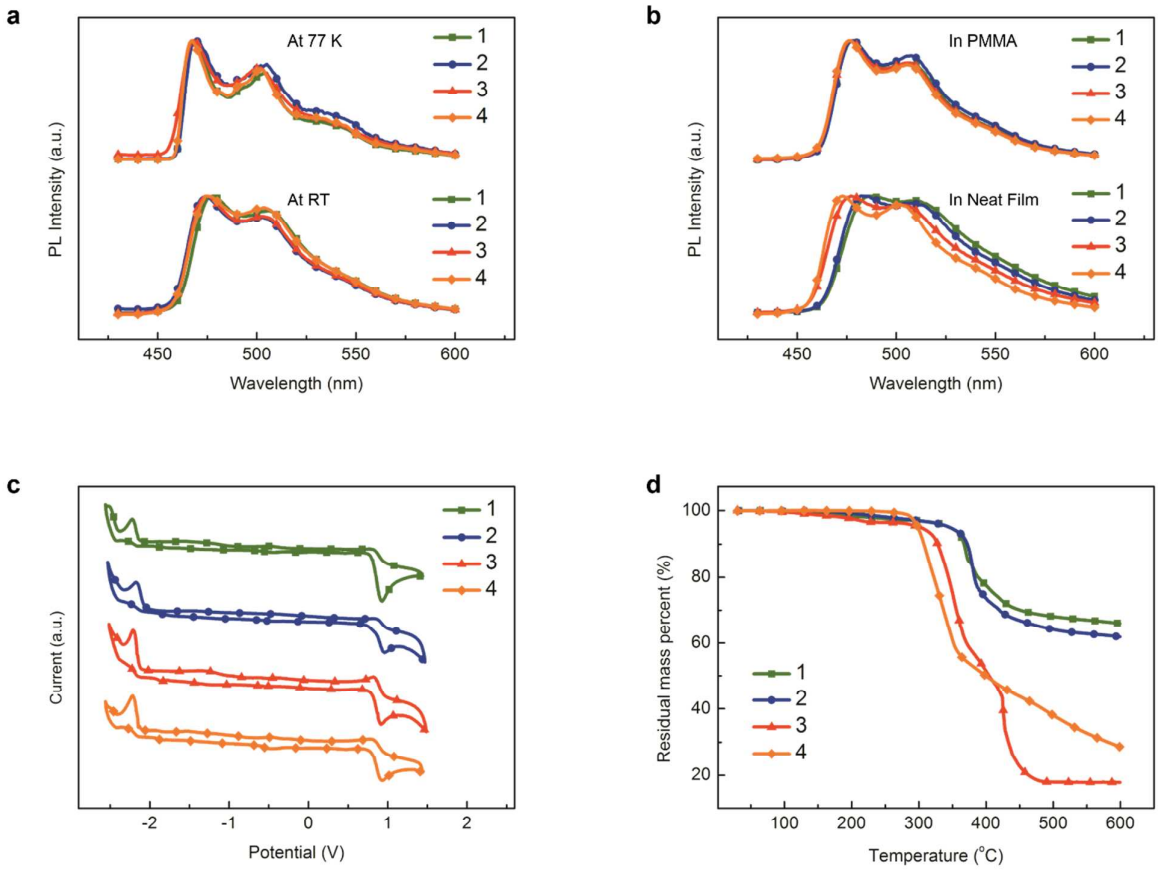

Figure 3. (a) Molecular structures and energy level diagram of materials used in OLEDs. Here PEDOT: PSS is poly (3,4-ethylenedioxythiophene): poly(styrene sulfonate), PVK is poly(*N*-vinylcarbazole) and OXD-7 is 1,3-bis(5-(4-*tert*-butylphenyl)-1,3,4-oxadiazol-2-yl)benzene. (b) PL spectra of the light-emitting layer and EL spectra of the optimized devices. (c) *J*-*V* and (d) *L*-*V* characteristics.

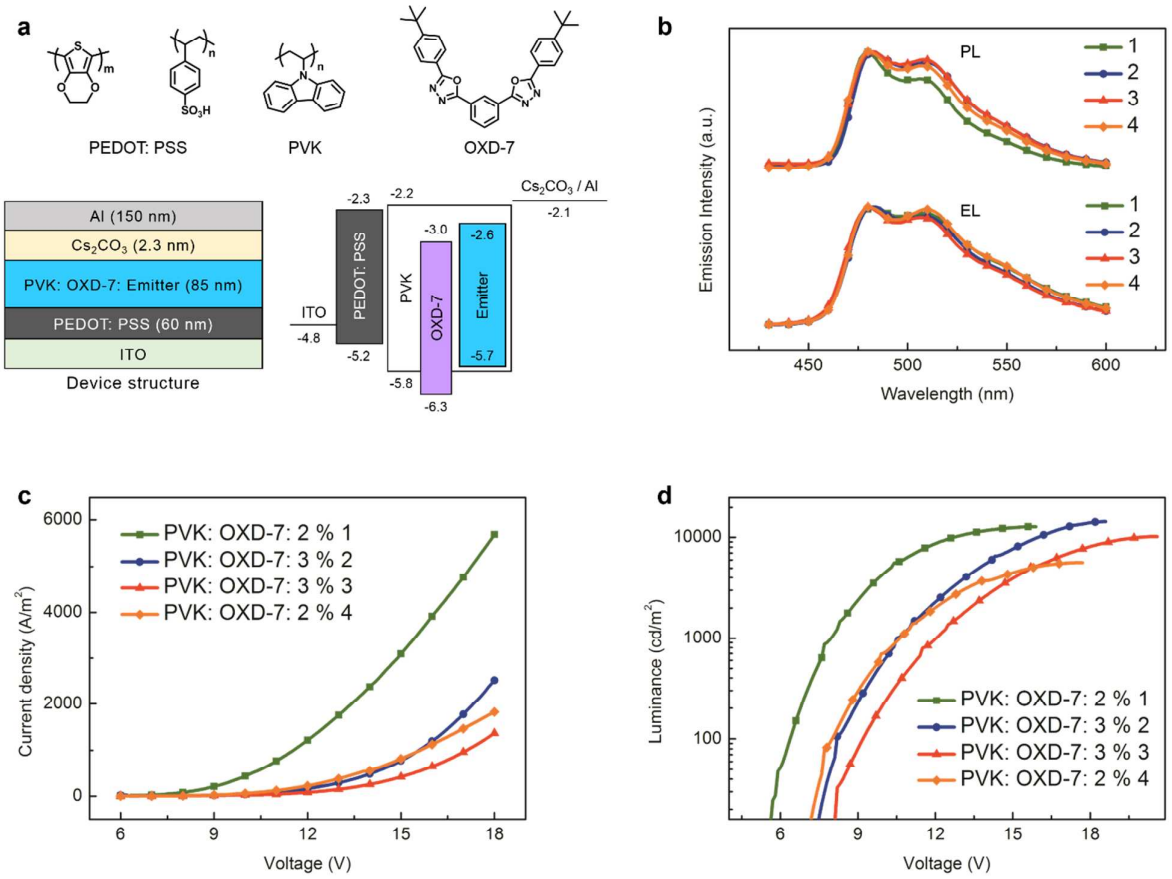

Figure 4. *J-V* of single-carrier devices based on complexes 1-4. The structure of hole-only device is ITO/ PEDOT: PSS (60 nm)/ PVK: OXD-7: *x* wt. % Emitter (85 nm)/ Al (150 nm), while that of electron-only device is ITO/ PVK: OXD-7: *x* wt. % Emitter (85 nm)/ Cs_2CO_3 (2.3 nm)/ Al (150 nm). Here *x* = 2 for complex 1 or 4, *x* = 3 for complex 2 or 3.

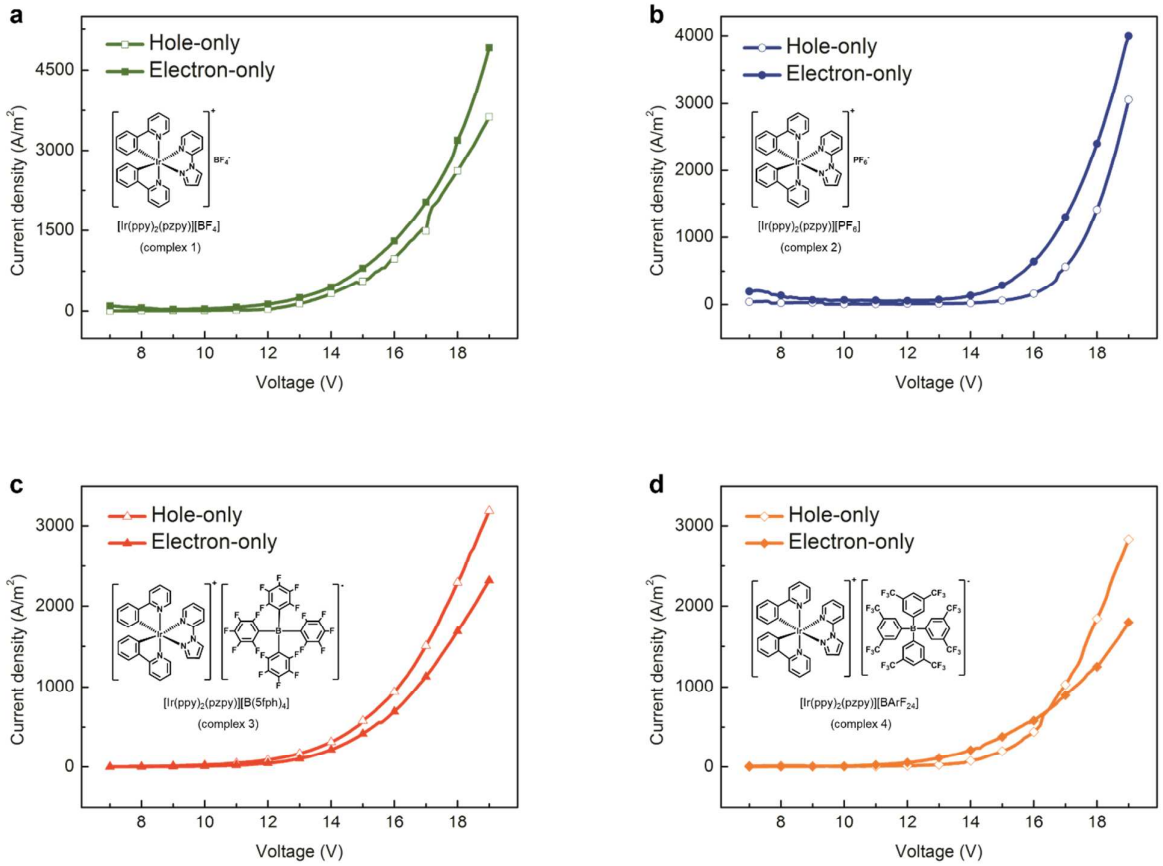

Figure 5. (a) Illustration of movement and redistribution of ions under an applied bias in devices with a structure of ITO/ PEDOT: PSS (60 nm)/ PVK: OXD-7: 20 wt. % Emitter (85 nm)/ Al (150 nm). (b) *J-V* and *L-V* (insert) characteristics of the devices.

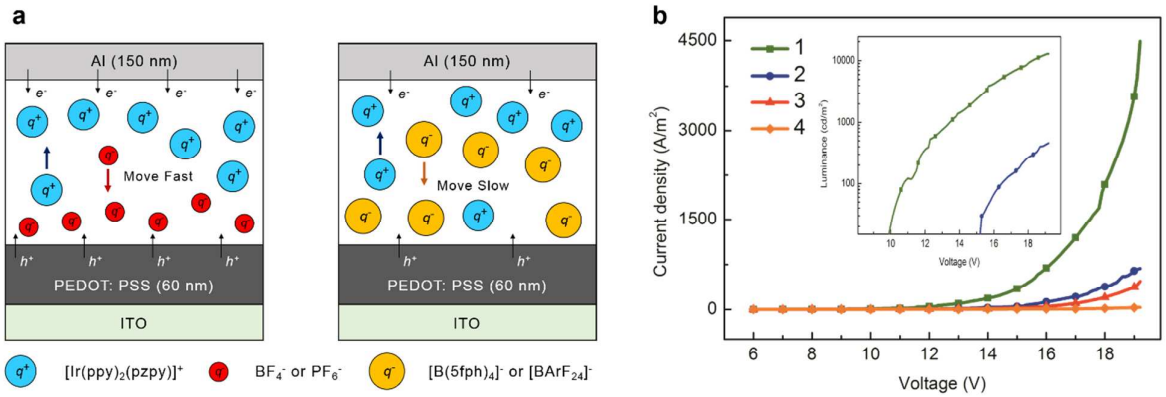

Table 1. Photophysical properties, electrochemical behaviours and thermal stability of complexes 1-4.

	Absorption	In solution		In PMMA	In neat film		At 77 K	Redox		$\Delta T_{5\,\%}$
	λ (nm)[b]	λ (nm)[c]	φ [τ (μs)][d]	λ (nm)[e]	λ (nm)[f]	φ [τ (μs)][g]	λ (nm)[h]	E_{ox}	E_{red}	(°C)[j]
	[ε ($\times10^4$ M^{-1} cm^{-1})]							(V)[i]	(V)[i]	
1	256 (5.02), 381	478, 506	0.19	479, 507	487, 507	0.02 [0.14,	469, 505 (sh),	0.87	-2.20	346
	(0.89)	(sh)	[1.58]	(sh)	(sh)	0.94 (8 %)]	535 (sh)			
2[a]	253 (5.51), 380	475, 503	0.23	478, 508	483, 504	0.03 [0.19,	469, 505 (sh),	0.88	-2.19	346
	(0.53)	(sh)	[1.56]	(sh)	(sh)	0.42 (12 %)]	535 (sh)			
3	254 (5.88), 379	475, 503	0.24	477, 506	476, 503	0.40 [0.45,	468, 502 (sh),	0.85	-2.18	320
	(0.45)	(sh)	[1.60]	(sh)	(sh)	1.02 (50 %)]	534 (sh)			
4	254 (5.23), 379	474, 503	0.27	476, 506	473, 502	0.39 [0.32,	467, 502 (sh),	0.87	-2.17	299
	(0.54)	(sh)	[1.56]	(sh)	(sh)	1.20 (73 %)]	534 (sh)			

[a] Originated from our previous work.[34] [b] In acetonitrile solution (1×10^{-5} M), ε denotes the molar extinction coefficients. [c] In degassed acetonitrile solution (2×10^{-5} M), *sh* denotes the shoulder wavelength. [d] The φ was measured *versus* quinine hydrogen sulfate with φ = 0.545 in 1 M H_2SO_4 (1×10^{-5} M). [e] Thin film with 5 wt. % doped in polymethylmethacrylate (PMMA). [f] Neat film about 100 nm thick, made on quartz substrates by spin-coating under air. [g] The percentage denotes the ratio of each lifetime. [h] In acetonitrile glass at 77 K in liquid nitrogen. [i] In degassed acetonitrile solution (1×10^{-3} M). Potentials were recorded *versus* the ferrocenium/ferrocence (Fc^+/Fc) couple. [j] The 5 % weight reduction temperatures were measured under nitrogen atmosphere.

Table 2. Detailed performance of solution-processed OLEDs doped with different concentrations of complexes 1-4.

	x^a	Φ^b	PL^c (nm)	Max CE^d (cd A^{-1}) (EQE)^d	Max L^e (cd m^{-2})	J at 15 V^f (A m^{-2})	EL^g (nm)	CIE^h (x, y)
1	2	0.30	479, 507 (sh)	14.8 (5.8 %)	12.5×10^3	3089	482, 508 (sh)	(0.23, 0.48)
	3	0.28	480, 508 (sh)	13.7 (5.4 %)	12.5×10^3	2471	482, 508 (sh)	(0.23, 0.48)
	5	0.20	480, 508 (sh)	11.0 (4.3 %)	10.7×10^3	2197	482, 508 (sh)	(0.23, 0.48)
	10	0.24	481, 508 (sh)	11.8 (4.6 %)	13.8×10^3	720	482, 508 (sh)	(0.23, 0.48)
	15	0.22	483, 508 (sh)	11.2 (4.4 %)	10.9×10^3	565	484, 508 (sh)	(0.23, 0.49)
	20	0.18	484, 508 (sh)	8.6 (3.4 %)	12.5×10^3	346	484, 508 (sh)	(0.24, 0.49)
	20^i	0.18	484, 508 (sh)	8.3 (3.3 %)	12.8×10^3	350	484, 508 (sh)	(0.23, 0.49)
2	2	0.25	482, 509 (sh)	12.0 (4.7 %)	10.6×10^3	1201	482, 508 (sh)	(0.21, 0.47)
	3	0.36	482, 509 (sh)	17.1 (6.8 %)	14.2×10^3	774	482, 508 (sh)	(0.21, 0.48)
	5	0.27	482, 509 (sh)	12.6 (5.0 %)	13.6×10^3	245	482, 508 (sh)	(0.21, 0.48)
	10	0.28	483, 509 (sh)	12.7 (5.0 %)	10.6×10^3	128	482, 508 (sh)	(0.21, 0.47)
	15	0.19	484, 507 (sh)	11.3 (4.5 %)	2.3×10^3	19	484, 506 (sh)	(0.21, 0.48)
	20	0.30	484, 509 (sh)	15.2 (6.0 %)	275	0.7	486, 508 (sh)	(0.20, 0.49)
	20^i	0.30	484, 509 (sh)	0.73 (0.29 %)	844	48	486, 508 (sh)	(0.20, 0.49)
3	2	0.27	482, 508 (sh)	13.1 (5.2 %)	12.9×10^3	424	480, 506 (sh)	(0.21, 0.46)
	3	0.29	482, 508 (sh)	13.6 (5.4 %)	10.2×10^3	420	480, 506 (sh)	(0.21, 0.46)
	5	0.15	482, 509 (sh)	9.0 (3.6 %)	7.3×10^3	396	480, 506 (sh)	(0.20, 0.46)
	10	0.17	482, 509 (sh)	9.5 (3.9 %)	5.9×10^3	59	482, 508 (sh)	(0.18, 0.44)
	15	0.16	483, 508 (sh)	9.3 (3.7 %)	2.8×10^3	32	480, 508 (sh)	(0.20, 0.46)
	20	0.22	483, 507 (sh)	9.9 (3.9 %)	1.4×10^3	10	486 (sh), 508	(0.20, 0.50)
	20^i	0.22	483, 507 (sh)	0.05 (0.04 %)	69	23	Not measured	
4	2	0.26	480, 507 (sh)	12.4 (4.9 %)	5.7×10^3	816	480, 508 (sh)	(0.21, 0.48)
	3	0.18	479, 505 (sh)	11.2 (4.4 %)	6.6×10^3	552	480, 508 (sh)	(0.19, 0.44)
	5	0.21	479, 508 (sh)	9.7 (3.8 %)	6.7×10^3	314	480, 508 (sh)	(0.21, 0.48)
	10	0.17	479, 507 (sh)	10.8 (4.3 %)	5.7×10^3	66	480, 508 (sh)	(0.21, 0.47)
	15	0.16	480, 508 (sh)	7.9 (3.1 %)	5.7×10^3	59	480, 508 (sh)	(0.20, 0.45)
	20	0.07	481, 509 (sh)	6.8 (2.7 %)	5.7×10^3	33	480, 508 (sh)	(0.21, 0.46)
	20^i	0.07	481, 509 (sh)	0.63 (0.25 %)	89	0.8	Not Measured	

[a] x, doping concentration. [b] Φ, PLQY of the corresponding light-emitting layer. [c] PL, photoluminescent wavelength. [d] CE, current efficiency; EQE, external quantum efficiency. [e] L, luminance. [f] J, current density. [g] EL, electroluminescence

wavelength. [h] *CIE*, Commission Internationale de I'Elairage. [i] Device with a structure of ITO/ PEDOT: PSS (60 nm)/ PVK: OXD-7: 20 wt. % Emitter (85 nm)/ Al (150 nm).

Table of Content

Highly efficient blue-green emitting diodes are attained by wisely controlling anionic migration of cationic iridium(III) complexes with different-sized counter-ions.